# IGLOO3D simulations of the 1st AIAA Ice-Prediction-Workshop database

Emmanuel Radenac, Quentin Duchayne

# IGLOO3D simulations of the 1st AIAA Ice-Prediction-Workshop database

Emmanuel Radenac*
Quentin Duchayne†
ONERA / DMPE, Université de Toulouse, F-31055 Toulouse - France

**This article presents the results of simulations performed at ONERA, with IGLOO3D and IGLOO2D, on the 1st-AIAA-Ice-Prediction-Workshop test cases. Except for the multi-element case for which the mesh could be refined at the level of the downstream elements, the trajectography seems accurately modeled. The accretion simulations give rather encouraging results considering that simple predictor or predictor-corrector simulations are performed. Avenues of progress such as the multi-step approach, the modeling of the ice density or the heat transfer are discussed.**

## Nomenclature

| | | |
|---|---|---|
| $c$ | = | Chord length, m |
| $C_p$ | = | Pressure coefficient, $C_p = (P - P_\infty) \,/\, \left(1/2\gamma P_\infty M_\infty^2\right)$ |
| $f_l$ | = | Liquid fraction of the accreted ice |
| $h_{tc}$ | = | Heat transfer coefficient, W/K/m$^2$ |
| $k_s$ | = | Equivalent sand-grain roughness height, m |
| $M$ | = | Mach number, $M = V/\sqrt{\gamma r T}$ |
| $P$ | = | Pressure, N/m$^2$ |
| $T$ | = | Temperature, K |
| $t$ | = | Exposure time to the icing cloud, s |
| $V$ | = | Velocity, m/s |
| AOA | = | Angle of attack, $^o$ |
| LWC | = | Liquid water content, kg/m$^3$ |
| MVD | = | Median volume diameter, m |
| $\beta$ | = | Collection efficiency, $\beta = \dot{m}/\left(\text{LWC} \cdot V\right)$ |
| $\phi$ | = | Heat flux, W/m$^2$ |
| *Subscript* | = | |
| $e$ | = | Edge of the boundary layer |
| $w$ | = | Wall |
| $\infty$ | = | Far-field |

*Research engineer, PhD, corresponding author: emmanuel.radenac@onera.fr
†Research engineer

# I Introduction

The AIAA 1st ice prediction workshop took place in July 2021. ONERA took part to this workshop, using both its 2D and 3D ice accretion suites, IGLOO2D[1] and IGLOO3D.[2,3] The workshop was dedicated to the investigation of both 2D and 3D ice-accretion test-cases, as well as collection efficiency assessment simply based on the computation of the water-droplet trajectories.

The goal of this article is to analyze the results obtained with ONERA's simulation tools on the workshop test-cases. Three kinds of data will therefore be compared with each other: experimental data, data from calculations with IGLOO2D and the results produced by the ONERA's 3D tools, IGLOO3D for the ice-accretion cases and CEDRE[8] for the collection-efficiency test-cases.

The numerical tools used for this article will be first briefly presented in section II. Then the test-cases related to droplet catch efficiency will be investigated in section III. Finally, sections IV and V will be dedicated to the ice-accretion test-cases, the 2D and 3D geometries, respectively.

# II Presentation of ONERA's numerical tools used during the workshop

## II.A Ice-accretion computational strategy

Both IGLOO2D and IGLOO3D rely on the standard quasi-steady method for ice-accretion simulations.[1,4,5] This approach consists of sequentially solving the airflow, the water-droplet trajectories and the thermodynamic balance for the water deposited on the icing surfaces. An ice-deposition mass-rate is produced by this succession of simulations. An ice-shape is inferred from this mass-rate, which changes the fluid volume. Several strategies can be employed for periodically modifying the fluid volume used for the airflow, water-droplet and ice computations.

For this article, the main strategy consisted in using the basic "predictor" approach, also known as "single-step" or "single-shot" approach in other workflows. For this approach, a single loop is run, based on the sequential call to the different codes, as described earlier. The ice-deposit deformation is thus directly computed from the ice-deposition-mass rate produced by the code and the time $t$ of the whole accretion process. The so-called "predictor-corrector" approach described in Trontin's article[1] was also used for this paper. This approach consists in running a second loop for which the airflow and droplet trajectories are computed around the predicted ice shape, and correcting the computation of the ice-deposition-mass rate thanks to this simulation. For this approach, it is thus necessary to generate a mesh around the predicted ice shape. It would be possible to make some "multi-step" simulations, especially for IGLOO2D because the computational time is low: the whole accretion-process time $t$ is divided into $N$ steps, allowing to run $N$ successive "predictor-like" loops. At the end of each loop, the ice shape is deformed according to a time of deformation $t/N$ and a new mesh is generated around this shape at the beginning of the following loop. However, this multi-step approach was not retained for the present article.

## II.B IGLOO2D

IGLOO2D[1] is ONERA's 2D icing suite, which allows to simulate all the necessary steps for an ice-accretion calculation, from the meshing to the computation of droplet trajectories and ice-accretion. Although features for modeling Appendix O and P icing conditions are also available in IGLOO2D, only Appendix C models will be used in this article.

The standard approach was used for the simulations of this article. Structured meshes were generated with the module *STRMESH2D* except for the case 121 (multi-element airfoil), for which an unstructured grid was generated with *gmsh*.[6] The airflow simulations were run with the inviscid *EULER2D* code, coupled to the boundary-layer solver *SIM2D* (simplified integral method). As regards the simulation of the droplet trajectories, the Lagrangian solver *TRAJL2D* was employed. For the thermodynamic balance on the iced surface, the Messinger solver *MESSINGER2D* was used.

The simulations were systematically performed with standard options, allowing for instance:

- full deposition of droplets (since only Appendix C simulations were run),
- the use of the Schiller and Naumann model for the droplet drag,
- the use of a laminar-turbulent transition on rough wall (abrupt transition governed by Braslow's criterion),
- the computation of a heat transfer coefficient given by Smith and Spalding's model in the laminar area and by a model similar to the one of Kays and Crawford in the turbulent area,
- the use of an ice density given by the model of Makkonen and Stallabras,[7] etc.

The interested reader will find further information in Trontin's article.[1]

For "infinite-like" swept wings such as the ones investigated in the 3D ice-accretion test-cases, the input Mach number for IGLOO2D, $M_{\infty,2D}$ was corrected by the sweep angle $\Lambda$: $M_{\infty,2D} = \cos(\Lambda)M_{\infty}$ (and the angle of attack could be slightly changed to adjust the pressure profile).

### II.C IGLOO3D

Contrary to IGLOO2D, the ONERA's 3D ice-accretion suite IGLOO3D[2,3] is mainly modular. The main solver of the icing suite IGLOO3D is the thermodynamic ice-accretion solver MESSINGER3D, based on Messinger's approach for the thermodynamic balance regarding the water deposited on the icing surfaces. The approach consists in applying the basic Messinger balance of mass and energy along the friction lines. Since the icing surfaces are divided into control volumes, the fluxes are computed along each edge of the volumes such that the balance is met along the lines parallel to the skin friction field. Besides, IGLOO3D allows different solvers to communicate with each other in order to achieve all the steps necessary for ice-accretion simulations. The solvers are coupled with each other through CGNS file inputs and outputs. In particular, for this article, the CEDRE solvers for the airflow and droplet-trajectory simulations will be used. These solvers will be presented in the next section. In previous articles,[2,3] other solvers could also be used, such as elsA for the airflow computation for instance.

The grids used for the IGLOO3D and CEDRE computations of this article are the ones which were provided by the Ice-Prediction-Workshop Committee. To be more specific, the unstructured meshes were used since CEDRE is an unstructured code.

It must be specified that after the airflow simulations, the heat transfer coefficient, which plays a key role in glaze ice shape modeling, was computed thanks to the following formula:

$$h_{tc} = \frac{\phi_w}{T_w - T_r} \tag{1}$$

where $\phi_w$ is the wall heat flux produced by the airflow solver, $T_w$ is the wall temperature imposed as a boundary condition to the airflow solver and $T_r$ is the recovery temperature, classically modeled as follows:

$$T_r = T_e \left(1 + Pr^{1/3}\frac{\gamma - 1}{2}M_e^2\right), \tag{2}$$

under the assumption of turbulent regime, where $M_e$ is the isentropic Mach number (Mach number at the edge of the boundary layer if the total pressure is assumed constant in the flow outside of the boundary layer), $T_e$ is the air temperature outside of the boundary-layer (actually reconstructed from the assumed conservation of the total temperature in the flow outside of the boundary layer). $Pr = 0.7$ is the Prandtl number of air, $\gamma = 1.4$ is the ratio of heat capacities for air.

In addition, it was possible to activate a laminar-turbulent transition model for the 2D cases. This model consists in computing the heat transfer coefficient differently in the laminar area. First, the laminar area is identified as the region in which

$$\frac{k_s V_e}{\nu_e} \leq 600 \tag{3}$$

where $k_s$ is the equivalent sand-grain roughness height, which will be discussed later, $V_e$ is the edge velocity, which is directly linked to the Mach number $M_e$, and $\nu_e$ is the kinematic viscosity of the airflow. This is

a simple version of sharp transition based on Braslow's criterion. Second, the heat transfer coefficient is computed after Smith and Spalding's formula, as in IGLOO2D.[1]

Regarding the ice density, several options are available. The first option consists in using the same model as in IGLOO2D, after the model proposed by Makkonen and Stallabras.[7] For a second option, not employed in this article, the density is constant.

### II.D CEDRE

CEDRE is a multi-physics numerical tool, including unstructured solvers for several physical problems (airflow simulations, droplet trajectories, conductive heat transfer, radiative heat transfer,...).[8]

Among these solvers, the airflow solver CHARME was used,[8,9] as well as the Eulerian droplet-trajectory solver SPIREE.[10–12] Both CHARME and SPIREE are based on the finite volume method on unstructured grids. The Lagrangian droplet-trajectory solver SPARTE[10,13] was also employed for a few simulations.

Regarding CHARME, various numerical options are available for the space and time discretization and for the turbulence modeling for instance. For the simulations of this paper, the $k$-$\omega$ SST model was used for turbulence modeling, along with the model developed by Aupoix for modeling rough walls[14] whenever necessary. For this model, a constant wall temperature is imposed and the equivalent sand-grain roughness height was set to a constant value:

$$k_s = L/1000, \tag{4}$$

where $L$ is a reference length. For 2D airfoils, it is common practice in ONERA's codes to set $L$ equal to the chord length. For 3D objects, it is less obvious to link the roughness height to a unique reference length, and the validity of the empiric correlation (4) is questionable. Nevertheless, this relation was used because swept airfoils are investigated and it is still possible to define an equivalent chord length. It must be mentioned that for the collection-efficiency test-cases, it was not deemed necessary to activate any rough-wall modeling since the wall roughness mainly affects the heat transfer and the skin friction at the walls rather than the airflow and droplet trajectories.

Regarding the numerical schemes, a second-order space discretization was used based on the HLLC scheme and a MUSCL reconstruction. For the time discretization, a basic first-order Euler implicit scheme is used with local time-stepping, since the steady-state solution is sought. The CFL numbers employed reach around 10 to 50 according to the test-case investigated. The system is solved with a GMRES method.

As regards SPIREE, the Schiller and Naumann model was used for the drag modeling. Full deposition is assumed on walls because only the Appendix C test-cases were investigated. As in CHARME, a first-order Euler implicit scheme is used with local time-stepping, and the GMRES method is used. A second-order space discretization is also used, based on a Godunov-like scheme[10] and a MUSCL reconstruction.

Note that the same drag model was used with SPARTE.

## III Collection-efficiency test-cases

### III.A Subset of cases addressed

The cases defined as "baseline" were addressed for this workshop. The flow conditions are given in table 1. A 27-bin droplet size distribution was provided by the organizing committee for cases 121 and 111. The interested reader can find further information in the article summarizing the outcomes of the Ice-Prediction-Workshop.[15] There was no liquid water content (LWC) provided for the collection efficiency test-cases. Since only the non-dimensional quantity of deposited water (collection efficiency $\beta$) is sought, the value of the LWC does not affect the results. LWC was thus set to an arbitrary value, 1 g/m$^3$.

| Case | AOA ($^o$) | $V_\infty$ (m/s) | $P_\infty$ (Pa) | $T_\infty$ (K) | MVD ($\mu$m) | LWC (kg/m$^3$) |
|---|---|---|---|---|---|---|
| Case 121 | 4 | 78.2 | 95630 | 278 | 21 | $10^{-3}$ |
| Case 111 | 6 | 78.68 | 95147 | 280 | 21 | $10^{-3}$ |

**Table 1:** *Collection efficiency cases investigated*

### III.B Case 121: Multi-element airfoil case

Figure 1 both shows the geometry of the multi-element airfoil and the pressure coefficient on the three elements, slat, main element and flap. There is no experimental pressure measurement available for the angle of attack of this simulation. So it is only possible to compare between the results of the two codes, IGLOO2D and IGLOO3D. The approaches used for the two codes are very different:

- the airflow is computed with an inviscid approach for IGLOO2D and a RANS approach for IGLOO3D;
- the grid is thus much coarser for IGLOO2D than for IGLOO3D.

However, there is a rather good agreement between IGLOO2D and IGLOO3D, especially on the pressure side of the three elements. The discrepancies are mainly obtained on the slat (especially in the cove).

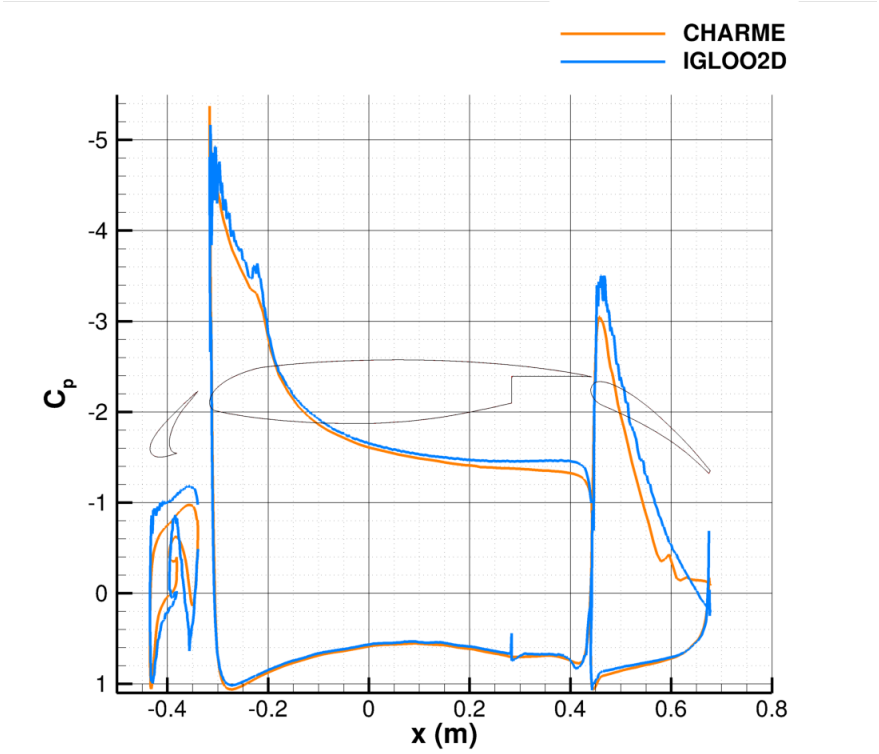


**Figure 1:** *Case 121, multi-element airfoil. Pressure coefficient produced on the three elements by CHARME and EULER2D.*

Again, the approaches retained for the computation of droplet trajectories in the two codes have major differences. First, the airflow which drives the droplets is computed differently, as discussed earlier. Second, a Lagrangian method is used for IGLOO2D, whereas a Eulerian approach is used for IGLOO3D. The Eulerian approach is known to be either much cheaper than the Lagrangian approach or easier to run, especially in 3D. Indeed, the Lagrangian simulations require to find a trade-off on the number of transported droplets, in order to ensure a good accuracy for a reasonable computational time (even in 2D, transporting all the physical droplets of the cloud would be too costly). For this simulation, 10000 particles were employed per bin, which requires to restrict the droplet injection area in the zone of interest only (injection of only

the droplets that impact on the wing). This is not necessary for Eulerian codes. However, there are some drawbacks for Eulerian codes. For instance, it is more difficult to deal with droplet re-emission when there is some rebound or splashing at the wall. This should not be an issue here since only Appendix C cases are addressed and no complex impact is thus expected. Another issue is that numerical dissipation can be experienced in Eulerian codes. This should especially be a problem for the elements located downstream, because the issue can be encountered especially in the wake area.

Figures 2a and 2b show the collection efficiency on the slat, as produced by both CEDRE and IGLOO2D, respectively for the 27-bin droplet-size distribution provided by the committee and for the classical Langmuir-D droplet-size distribution. The results for the Langmuir-D distribution look slightly better on the slat than for the 27 bin distribution, which may be fortuitous.

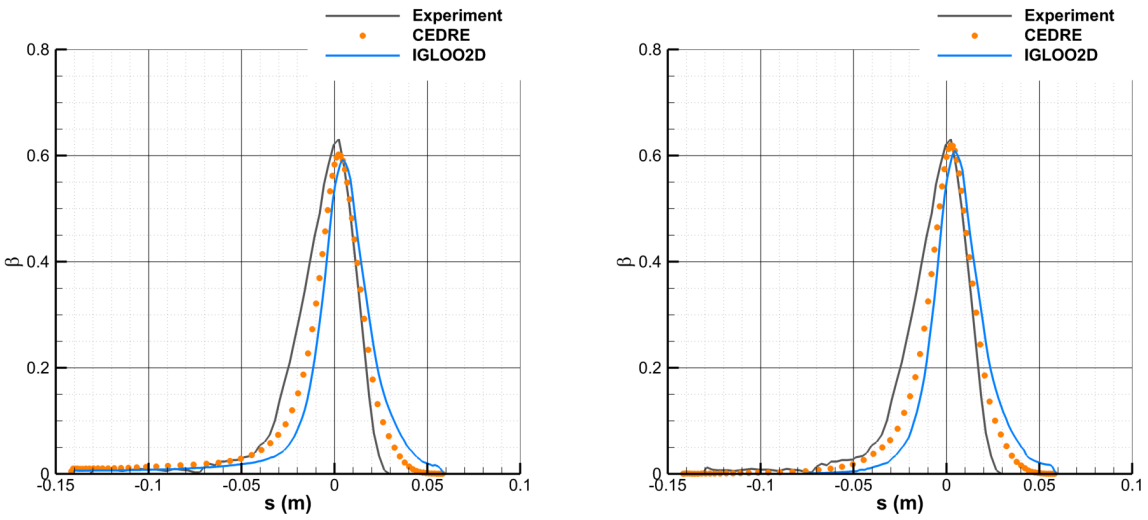


**(a)** *27-bin baseline droplet-size distribution*

**(b)** *Langmuir-D droplet-size distribution*

**Figure 2:** *Case 121, multi-element airfoil. Collection efficiency on the slat, produced by SPIREE and TRAJL2D.*

This is indeed not observed further downstream on the main element (figure 3) and on the flap (figure 4). The main conclusion which can be driven for both elements is that the $\beta$ peaks are lower for CEDRE than for IGLOO2D. The reason for that is actually an effect of numerical dissipation. Simulations performed with the Lagrangian solver SPARTE instead of SPIREE indeed tend to grow the peak value of $\beta$ as shown in figure 5. This is verified from the slat (slight increase in $\beta_{max}$, around 5 %), but it is even more remarkable for the subsequent elements (main element, 15 % increase, and flap, 35 % increase). It would thus be beneficial for the Eulerian approach to ensure a good level of refinement of the meshes used for the computation around multi-element airfoils. For the first element or for single elements, the baseline grid looks quite sufficient, but for further elements, the peak value of $\beta$ is too strongly reduced by numerical dissipation.

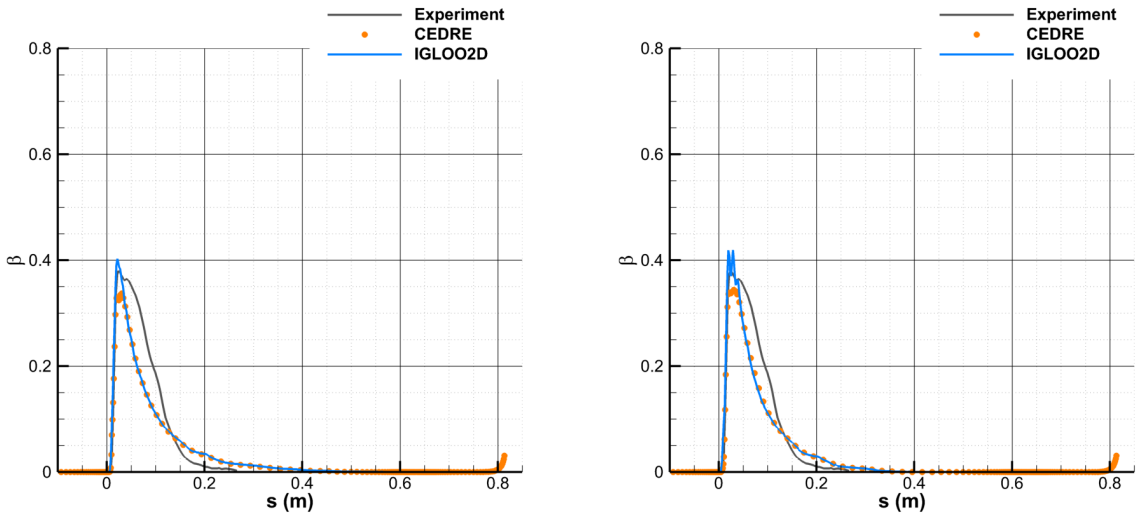


**(a)** *27-bin baseline droplet-size distribution* **(b)** *Langmuir-D droplet-size distribution*

**Figure 3:** *Case 121, multi-element airfoil. Collection efficiency on the main element, produced by SPIREE and TRAJL2D.*

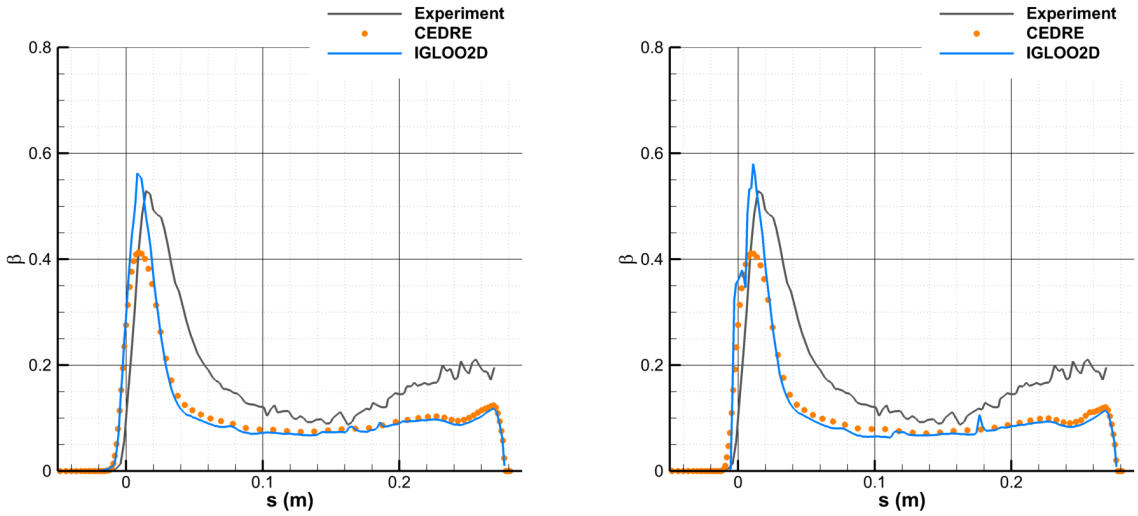


**(a)** *27-bin baseline droplet-size distribution* **(b)** *Langmuir-D droplet-size distribution*

**Figure 4:** *Case 121, multi-element airfoil. Collection efficiency on the flap, produced by SPIREE and TRAJL2D.*

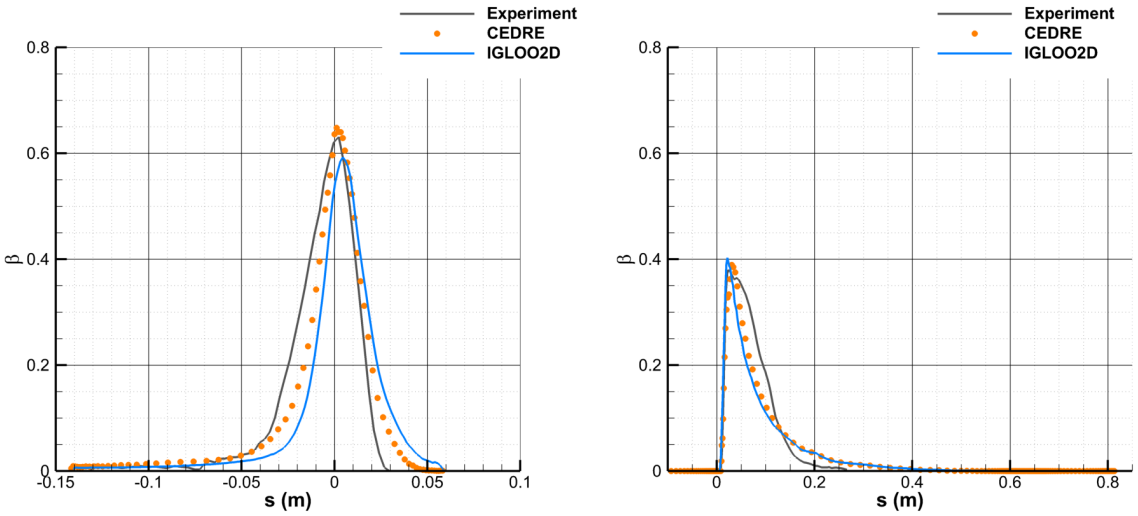


**(a)** *Slat*

**(b)** *Main element*

**(c)** *Flap*

**Figure 5:** *Case 121, multi-element airfoil, 27-bin baseline droplet-size distribution. Collection efficiency on the main element, produced by SPARTE and TRAJL2D.*

### III.C Case 111: NACA 64A008 finite swept tail

Case 111 is a case for which pressure and collection efficiency measurements are available on a swept airfoil (single body). Figure 6a shows that the pressure coefficient is correctly captured by the solver CHARME. For the sake of clarity, only the pressure coefficient on the so-called inboard cut is shown but the agreement between simulations and experiment is very good on the outboard cut too.

Regarding the collection efficiency, the agreement between the measured $\beta$ and the simulations with SPIREE and SPARTE is very good (figure 6b). This test-case confirms that the use of the meshes provided by the organizing committee are sufficienlty refined for the Eulerian approach not to produce a noticeable numerical diffusion on a single element. The agreement between the Eulerian SPIREE solver and the Lagrangian SPARTE solver is indeed excellent (the agreement is even better than for the slat of test-case 121).

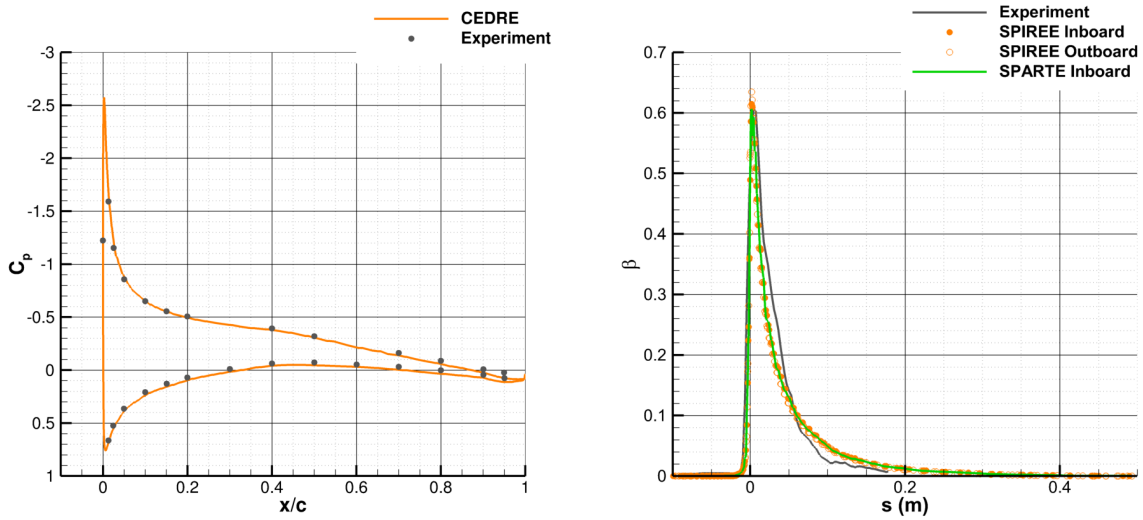


**(a)** $C_p$ **(b)** $\beta$

**Figure 6:** *Case 111, finite swept tail. Pressure coefficient on the inboard section, collection efficiency produced by SPIREE and SPARTE.*

## IV 2D ice-accretion test-cases

### IV.A Subset of cases addressed

The cases defined as "baseline" were addressed for this workshop. Table 2 shows the icing conditions for these cases, for which a NACA23012 airfoil is used.

Only the rime-ice baseline case (case 241) will actually be analyzed in the present paper. The glaze-ice baseline case (case 242) indeed showed a wide spread in the results produced by the various codes used by all the participants to the Ice-Prediction-Workshop. Case 242 has very similar icing conditions as condition number 5 in Trontin's article.[1] For condition number 5, the numerical results were rather poor in terms of horn size and horn angle. Some further investigation on the use of multi-stepping and alternative models for instance would thus be necessary. These investigations have not been done yet and there is no interest in addressing this case in the present paper. The interested reader is referred to the synthesis paper of the workshop[15] for further information both about the input data and about case 242 results.

A 7-bin droplet size distribution was provided by the organizing committee for case 241. After equation (4), the equivalent sand-grain roughness height employed for the computation is $k_s = 0.4572$ mm.

| Case | $c$ (m) | AOA ($^o$) | $V_\infty$ (m/s) | $P_\infty$ (Pa) | $T_\infty$ (K) | MVD ($\mu$m) | LWC (kg/m$^3$) | $t$ (s) |
|---|---|---|---|---|---|---|---|---|
| Case 241 | 0.4572 | 2 | 102.889 | 92528 | 250.15 | 30 | $0.42 \cdot 10^{-3}$ | 300 |

**Table 2:** *2D ice-accretion cases investigated*

### IV.B Case 241: 18-in NACA23012 airfoil, rime ice

As shown in figure 7, there are no major differences between the ice shapes produced by the two droplet-size distributions assessed, i.e. the baseline distribution provided by the organizing committee and the classical Langmuir-D distribition. Besides, there are quite interesting conclusions to be drawn. First, the agreement between IGLOO2D and IGLOO3D is very good in predictor approach (single-step ice accretion simulation). Second, the predictor-corrector approach assessed with IGLOO2D produces a rather satisfactory ice shape, compared to the experimental one.

In rime-ice regime, the ice shape is directly linked to the collection efficiency because the water freezes locally. Figure 8a shows that there is a perfect agreement between the collection efficiency produced by IGLOO2D and IGLOO3D on the clean airfoil (which confirms the rather good agreement obtained on the slat for case 121). It is thus logical that the ice shapes are also correctly captured for both codes.

The ice shape is slightly chaotic in the vicinity of the stagnation point for IGLOO3D. This is due to the fact that there is a little bit of runback due to locally low values of heat transfer coefficient. Indeed, figure 8 shows that the liquid fraction is not zero close to the stagnation point, where the heat transfer coefficient $h_{tc}$ approaches 0 (on the clean airfoil). This very low value of $h_{tc}$ at the stagnation point is not expected. It is mainly due to the fact that the grid is slightly finer in the streamwise direction than for IGLOO2D (figure 9). Apart from this error at the stagnation point, the agreement on $h_{tc}$ can be judged as quite satisfactory between the two codes. The agreement is even very good, considering the fact that very different approaches are used between the two codes (viscous-inviscid coupling for IGLOO2D vs. Navier-Stokes approach for IGLOO3D, the rough-wall-effect modeling is thus also handled differently). By the way, the spreading in the results of the two codes on $h_{tc}$ is also much smaller than the dispersion observed between all the codes of the workshop.[15]

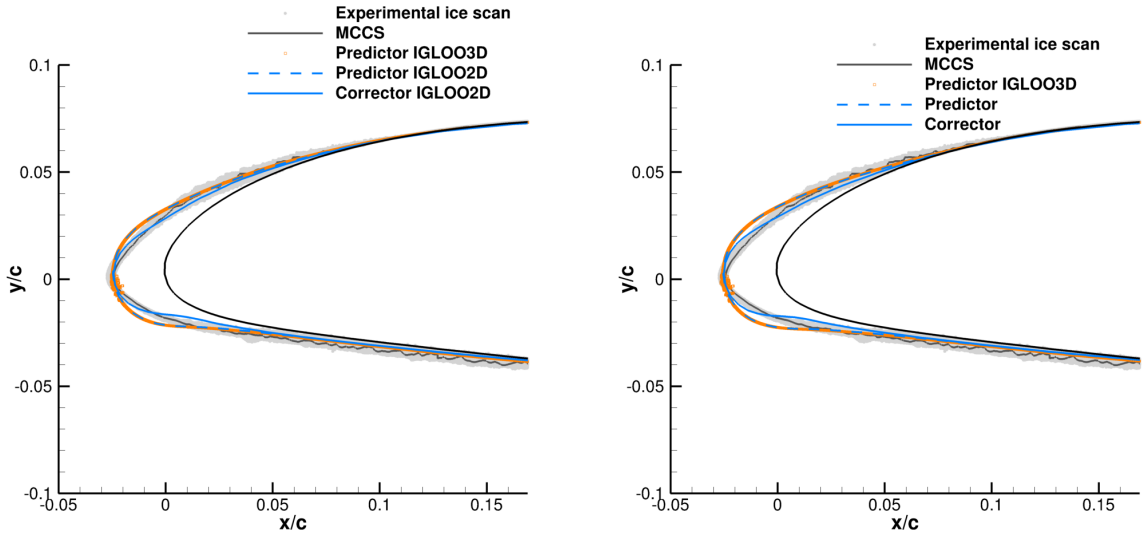


**(a)** *7-bin baseline droplet-size distribution* **(b)** *Langmuir-D droplet-size distribution*

**Figure 7:** *Case 241, 2D rime-ice case. Ice shapes produced by IGLOO2D and IGLOO3D. Comparison against the experimental ice shape.*

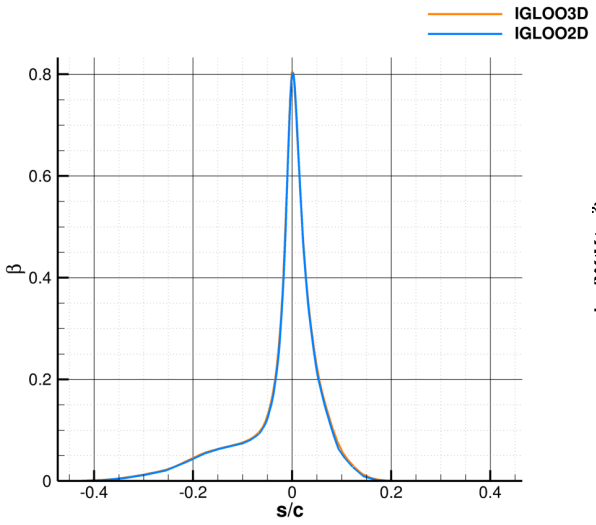


**(a)** $\beta$

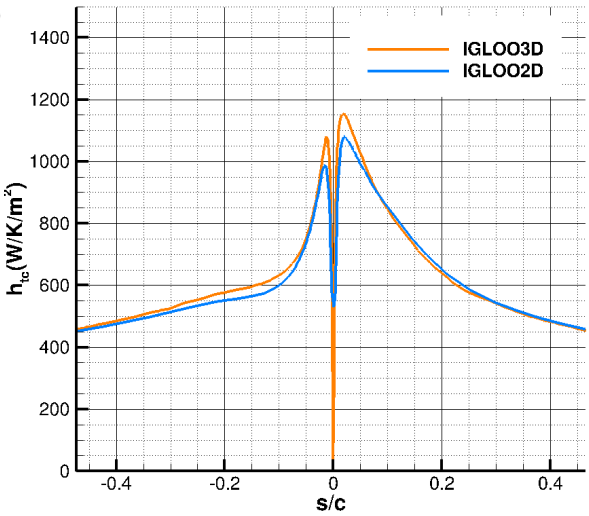


**(b)** $h_{tc}(W/K/m^2)$

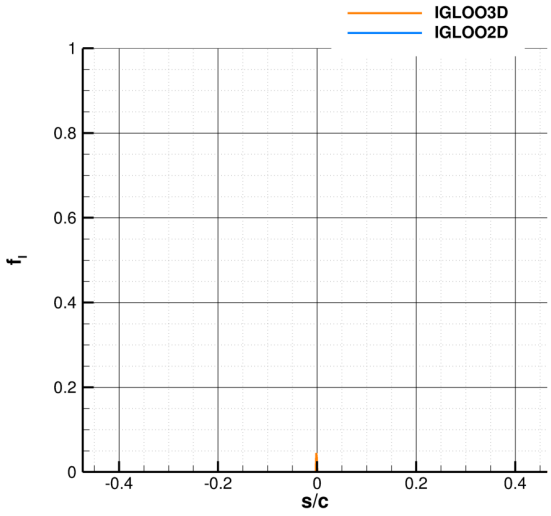


**(c)** $f_l$

**Figure 8:** *Case 241, 2D rime-ice case. Collection efficiency, heat transfer coefficient and liquid fraction produced by IGLOO2D and IGLOO3D.*

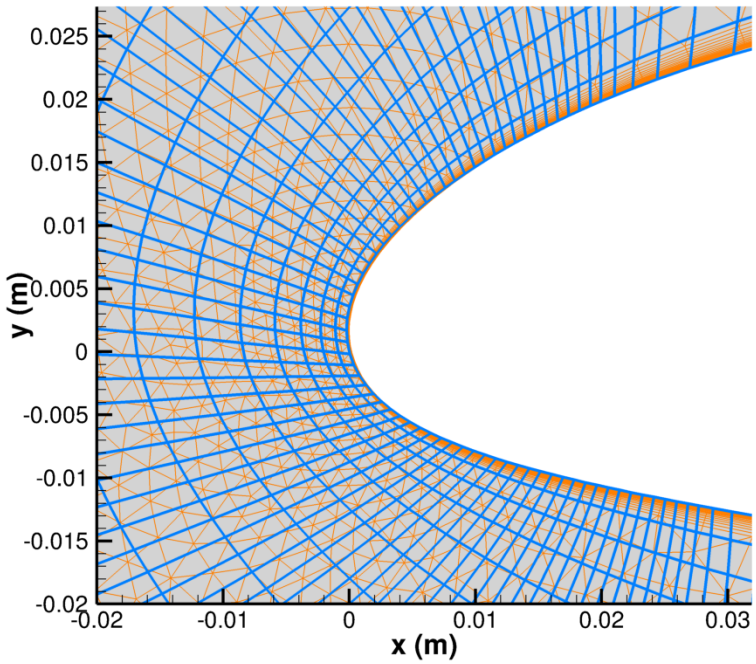


**Figure 9:** *Case 241, 2D rime-ice case. Comparison between the grids used for IGLOO2D (blue lines) and for IGLOO3D (orange lines).*

# V 3D ice-accretion test-cases

## V.A Subset of cases addressed

The cases defined as "baseline" were adressed for this workshop. Table 3 shows the icing conditions for the four test-cases investigated. NACA0012 airfoils are employed for all test-cases. Two different sweep angles are used, $30^o$ and $45^o$. Again, the interested reader will find further information in the synthesis paper of the workshop.[15]

The 7-bin droplet size distributions provided by the organizing committee were used for these cases. After equation (4), the roughness size was set to 0.91438 mm.

| Case | $c$ (m) | Sweep Angle ($^o$) | AOA ($^o$) | $V_\infty$ (m/s) | $P_\infty$ (Pa) | $T_\infty$ (K) | MVD ($\mu$m) | LWC (kg/m$^3$) | $t$ (s) |
|---|---|---|---|---|---|---|---|---|---|
| Case 361 | 0.91438 | 30 | 0 | 103 | 92321 | 257 | 34.7 | $0.5 \cdot 10^{-3}$ | 1200 |
| Case 362 | 0.91438 | 30 | 0 | 103 | 92321 | 266 | 34.7 | $0.5 \cdot 10^{-3}$ | 1200 |
| Case 371 | 0.91438 | 45 | 0 | 103 | 94463 | 257 | 32 | $0.5 \cdot 10^{-3}$ | 1200 |
| Case 372 | 0.91438 | 45 | 0 | 103 | 94463 | 266 | 32 | $0.5 \cdot 10^{-3}$ | 1200 |

**Table 3:** *3D ice-accretion cases investigated*

## V.B Case 361: $30^o$ sweep-angle NACA0012 airfoil, rime ice

For the rime ice case 361 with a $30^o$ sweep-angle NACA0012 airfoil, as shown in figure 10, the ice shape produced by the predictor approach is not so bad, compared to the experimental ice shape. The IGLOO2D and IGLOO3D predictor-corrector results do not even improve the ice shapes, which tend to be too sharp.

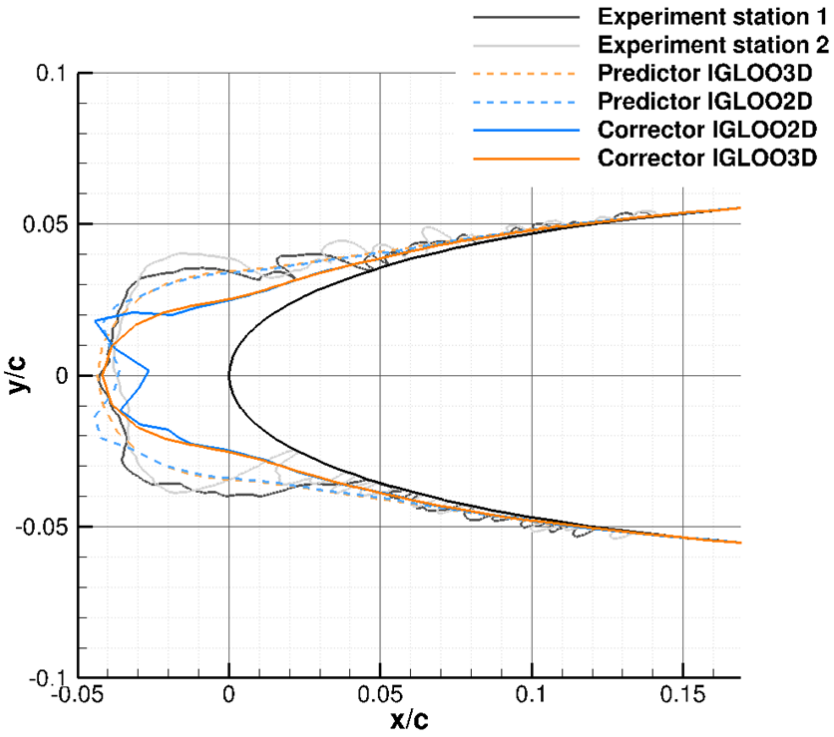


**Figure 10:** *Case 361, $30^o$ sweep-angle NACA0012 airfoil, rime-ice case. Ice shapes produced by IGLOO2D and IGLOO3D. Comparison against the experimental ice shape.*

It has to be noted that the use of a Langmuir-D ditribution instead of the 7-bin "baseline" distribution did not change much the ice shapes as shown in figure 11. The Langmuir-D distribution will thus no longer be assessed for the next test-cases. It is also worth noting that both IGLOO2D and IGLOO3D correctly capture the pressure coefficient distribution (figure 12a). Although overall, the two codes provide the same order of magnitude for the heat transfer coefficient $h_{tc}$, there are differences (figure 12b). In particular, $h_{tc}$ is larger for IGLOO3D, especially at the beginning of the profile where IGLOO2D provides a very small laminar zone and does not correctly accounts for the presence of a transverse flow. These small discrepancies are not enough to cause a major difference between the two codes on the ice shape. As long as the ice is "fully" rime and all the water freezes locally, the heat transfer indeed affects only the ice temperature. However, since IGLOO2D produces a low $h_{tc}$ at the stagnation point, there is a little bit of runback, which explains the small ice thickness reduction and the short horns further donwstream. The rest of the ice shape is directly linked to the water catch efficiency, for which the two codes produce very similar results as shown in figure 13a, and to the ice density. The only slight differences between the two codes as regards the water collection aspects concern the distribution of droplet sizes in the farthest downstream areas, where $\beta$ is very low (figure 13b). Regarding the ice density, both codes predict a value equal to 917 kg/m$^3$. The "predictor" ice shapes produced by the two codes are thus logically very similar.

In order to improve the results, it could be necessary to work on the ice density model. This model was proved to be rather satisfactory for 2D airfoils. However, the use of this model for 3D swept wings is more questionable. Also, if the ice shape exhibits a transverse pattern such as small scallops, it is unlikely that the predictor-corrector approach captures the shape, because the shadowing effects affecting the droplet collection are poorly modeled by this approach. A multi-step approach would be more appropriate.

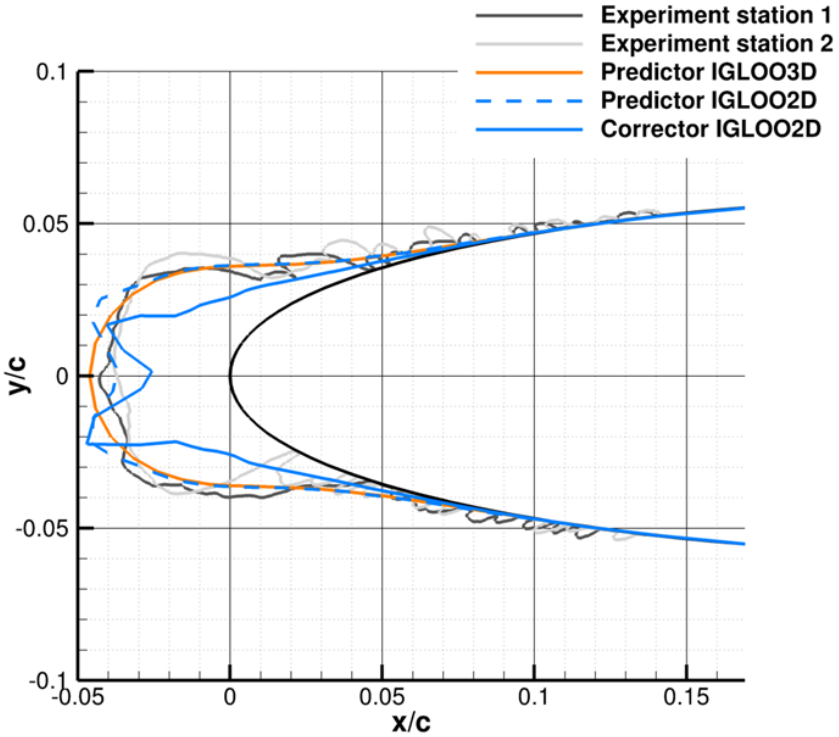


**Figure 11:** *Case 361, 30º sweep-angle NACA0012 airfoil, rime-ice case. Ice shapes produced by IGLOO2D and IGLOO3D with a Langmuir-D distribution. Comparison against the experimental ice shape.*

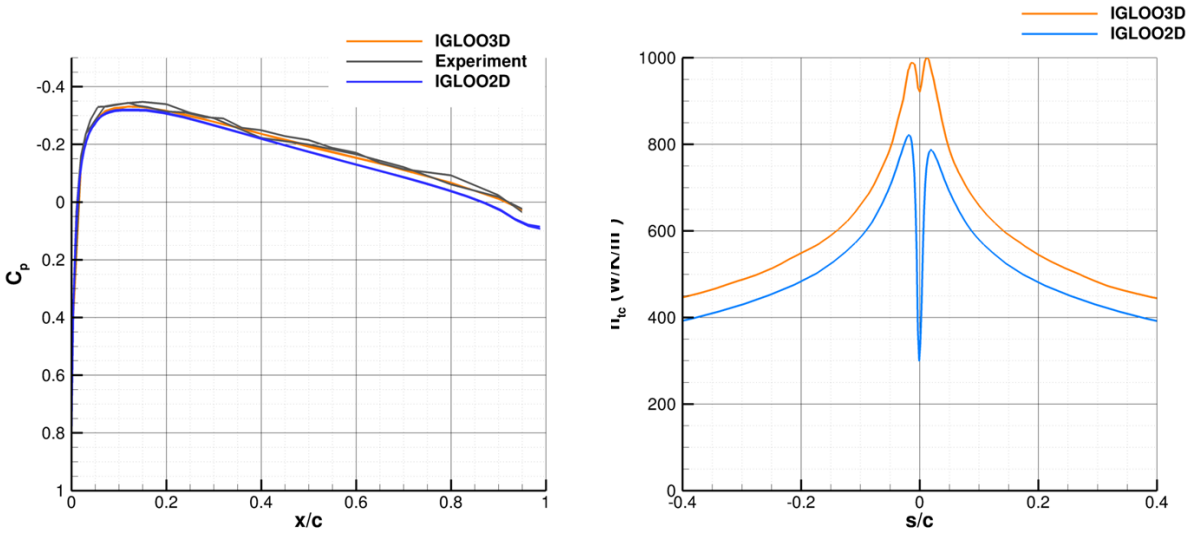


**(a)** $C_p$ **(b)** $h_{tc}(W/K/m^2)$

**Figure 12:** *Case 361, 3D rime-ice case. Pressure coefficient and heat transfer coefficient produced by IGLOO2D and IGLOO3D.*

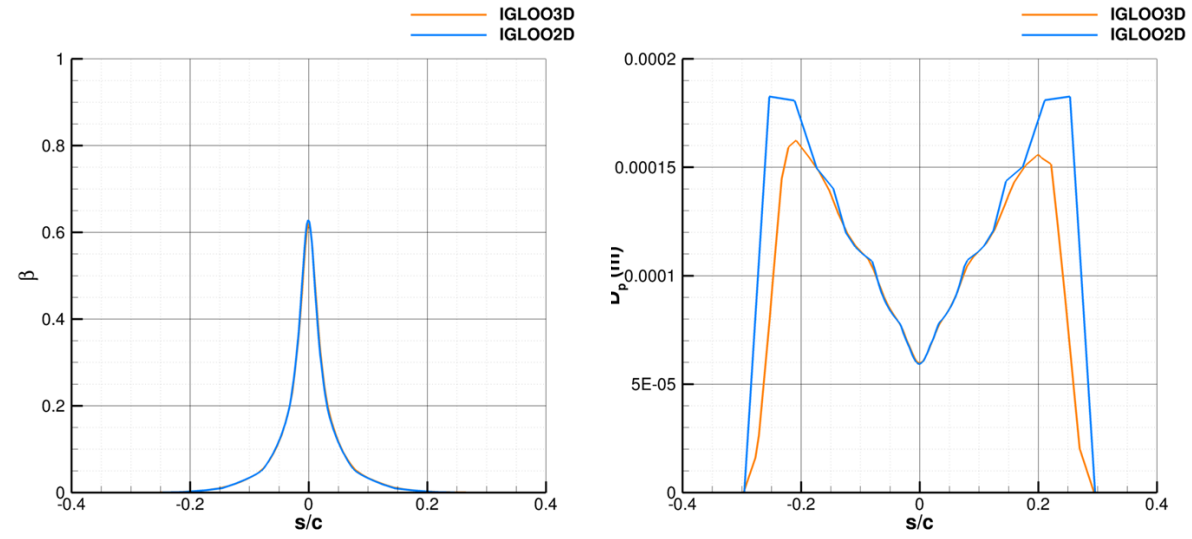


**(a)** $\beta$ **(b)** $D_{43}(m)$

**Figure 13:** *Case 361, 3D rime-ice case. Collection efficiency and droplet size produced by IGLOO2D and IGLOO3D.*

### V.C Case 362: 30$^o$ sweep-angle NACA0012 airfoil, glaze ice

For the glaze-ice case 362, figure 14 shows that the ice morphology is not captured by IGLOO2D and IGLOO3D.

The main avenue for improvement seems to concern the unsteady process. The predictor-corrector approach modifies the shape produced by IGLOO2D only marginally (figure 14). However, for IGLOO3D, this approach tends to flatten the ice shape along the separation line in a way very similar to the experimental shape. The horn heights are still not captured but this may be due to other aspects. First, as in case 261, the ice density model could be questioned and the use of a multi-step approach could help capturing some scallop-like patterns.

Second, it is possible that IGLOO3D produces too little runback, because $h_{tc}$ is high close to the stagnation point (as case 362 differs from case 361 only by the change of the air temperature, $h_{tc}$ has globally the same level as in figure 12b). This is due to the fact that for the swept-wings, it was not possible to activate a transition model in IGLOO3D and the boundary layer is thus fully turbulent. Modeling the laminar-turbulent transition would probably increase the amount of runback (and increase the liquid fraction to values similar to IGLOO2D, as shown in figure 15, or intermediate). However, it must be noticed that the ice thickness predicted by the IGLOO3D simulation is not so bad along the separation line. The ice thickness there is very good compared to the experimental shape. Therefore, the amount of runback should not be increased too significantly, otherwise the ice thickness at the stagnation point could be degraded.

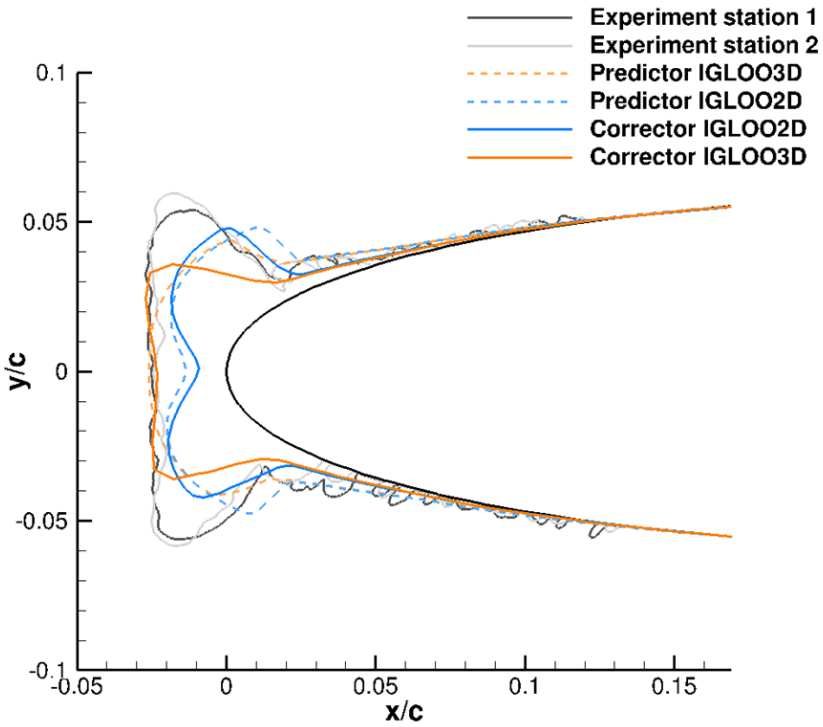


**Figure 14:** *Case 362, 30º sweep-angle NACA0012 airfoil, glaze-ice case. Ice shapes produced by IGLOO2D and IGLOO3D. Comparison against the experimental ice shape.*

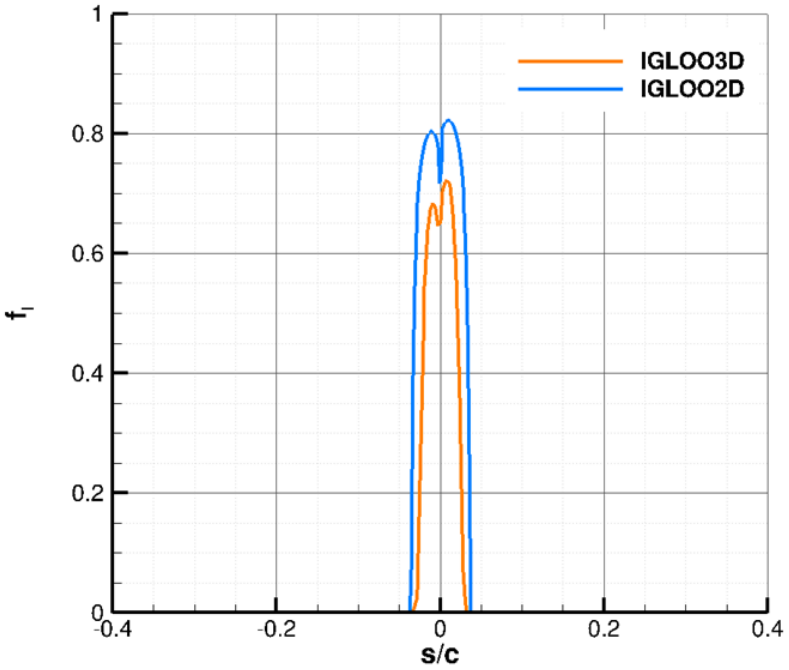


**Figure 15:** *Case 362, 30° sweep-angle NACA0012 airfoil. Liquid fractions produced by IGLOO2D and IGLOO3D.*

### V.D Case 371: 45$^o$ sweep-angle NACA0012 airfoil, rime ice

As shown in figure 16, the results for a 45$^o$ sweep-angle are worse than in the same condition for a 30$^o$ sweep-angle (case 361). The agreement between IGLOO2D and IGLOO3D is rather good. The main explanation for the slight discrepancies is that the heat transfer coefficient is predicted larger by IGLOO3D than by IGLOO2D (figure 17b), like in cases 361 and 362, the predictions of $\beta$ being again very similar (figure 17a). For the SUNSET2 database investigated in a previous article, there was the need to drastically change the ice density.[3] This could be done for test-case 371. However, the main issue is that the ice shape is too sharp, especially in predictor-corrector approach. For high sweep angles, various kinds of scallop-like ice shapes can be obtained.[16] The use of multi-step approaches could thus also help to better model the ice shape, as mentioned earlier.

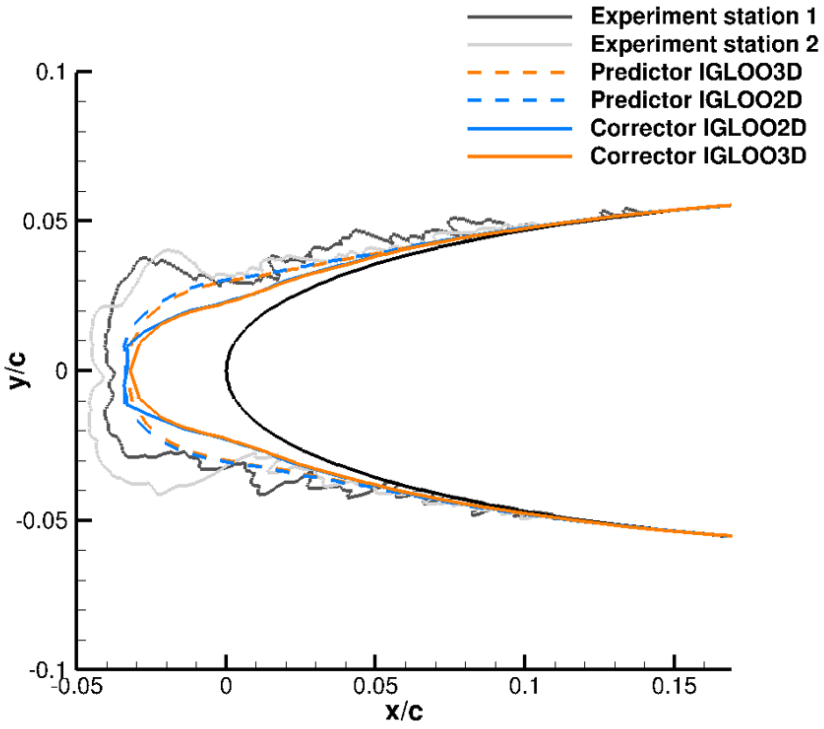


**Figure 16:** *Case 371, 45$^o$ sweep-angle NACA0012 airfoil, rime-ice case. Ice shapes produced by IGLOO2D and IGLOO3D. Comparison against the experimental ice shape.*

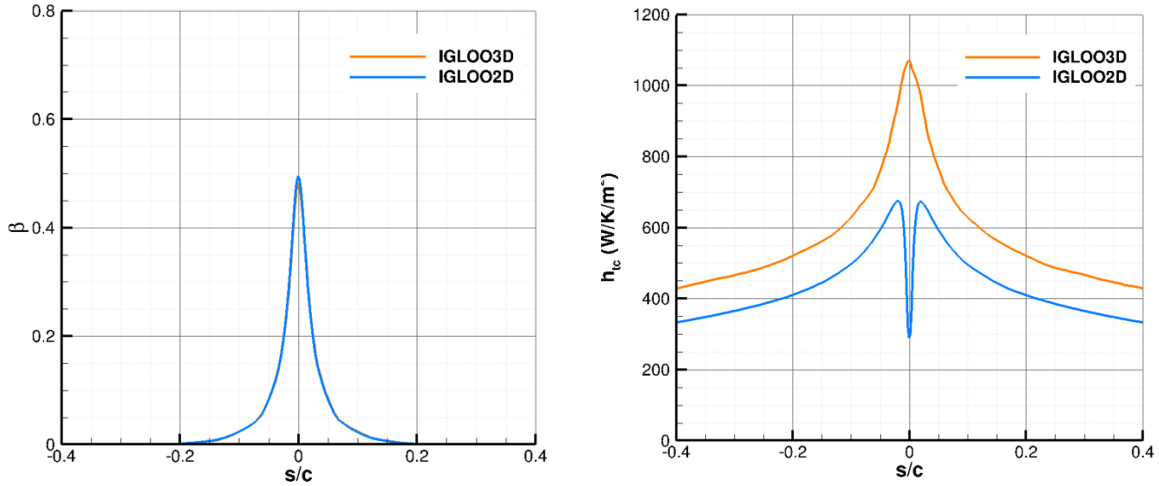


**(a)** $\beta$ **(b)** $h_{tc}$

**Figure 17:** *Case 371, 45° sweep-angle NACA0012 airfoil, 3D rime-ice case. Collection efficiency (baseline 7-bin distribution) and heat transfer coefficient produced by IGLOO2D and IGLOO3D.*

### V.E Case 372: 45$^o$ sweep-angle NACA0012 airfoil, glaze ice

The same conclusions hold for the glaze-ice case 372 as for the case 362 in the same icing conditions for a lower sweep angle (figure 18). Again, the ice morphology is not captured by IGLOO2D and IGLOO3D. The ice thickness predicted by the predictor IGLOO3D simulation is not so bad along the separation line. The ice thickness there is rather good compared to the experimental shape. However, the predictor-corrector approach does not improve the results, on the contrary. As in case 362, the use of a multi-step approach, the improvement of the heat transfer coefficient modeling (which mainly drives the amount of liquid-water runback) and the use of a better validated ice density could be interesting avenues for future progress.

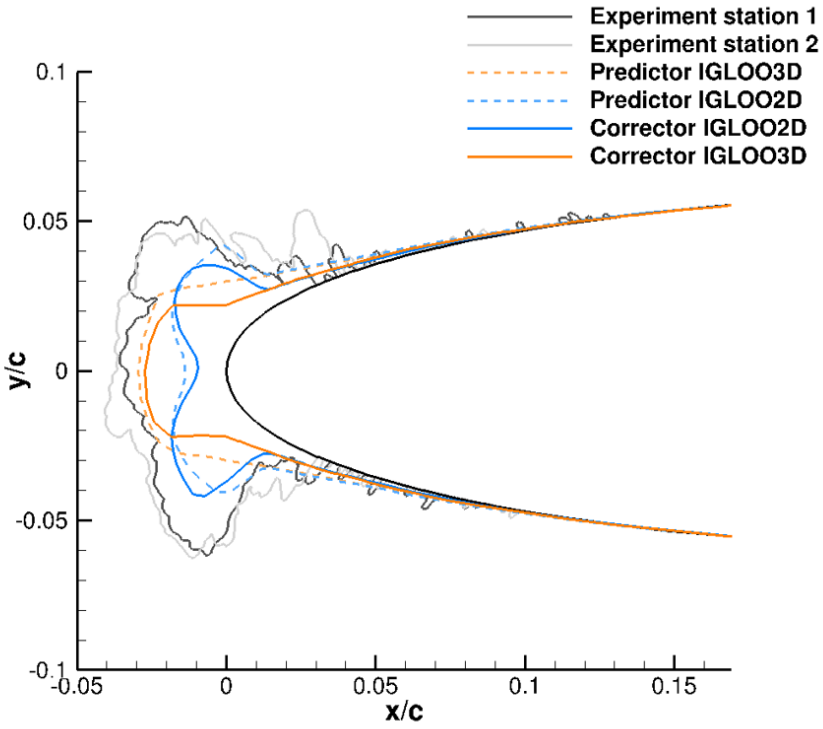


**Figure 18:** *Case 372, 45$^o$ sweep-angle NACA0012 airfoil, glaze-ice case. Ice shapes produced by IGLOO2D and IGLOO3D. Comparison against the experimental ice shape.*

## VI Conclusion

This article gives an overview of the simulations performed at ONERA for the first AIAA-Ice-Prediction-Workshop. All the baseline cases have been processed with ONERA's in-house tools, IGLOO3D and IGLOO2D. Rather encouraging results have been obtained. The collection efficiency of water droplets is overall rather well modeled, even if the Eulerian approach has shown some classical limitations on airfoils with several elements, which would require reworking the meshes for example. Regarding the ice accretion, on the cases shown, the results are often quite similar between the 2D code and the 3D code. The main source of difference concerns the heat transfer coefficient, which mainly affects glaze-ice shapes. It is interesting to note that the ice thickness on the separation line is rather well modeled by IGLOO3D, especially in the glaze-ice regime. However, the ice shapes on swept wings will require progress on the modeling of the unsteady growth of the ice in order to model the presence of scallops, as well as on the modeling of the ice density and that of the heat transfer coefficient.

## Acknowledgements

The authors would like to thank Thomas Renaud for the generation of some of the grids and his help, as well as Guillaume Jacquemart for his involvement in this study during his internship.

## References

[1] Trontin, P., Kontogiannis, A., Blanchard, G. and Villedieu, P. *Description and assessment of the new ONERA 2D icing suite IGLOO2D*, 9th AIAA Atmospheric and Space Environments Conference, AIAA AVIATION Forum, AIAA 2017-3417, 2017.

[2] Radenac, E. *Validation of a 3D ice accretion tool on swept wings of the SUNSET2 program.*, 8th AIAA Atmospheric and Space Environments Conference, AIAA AVIATION Forum, AIAA 2016-3735, 2016.

[3] Radenac, E., Gaible, H., Bezard, H., and Reulet, P., *IGLOO3D computations of the ice accretion on swept-wings of the SUNSET2 database.*, SAE Technical Paper 2019-01-1935, 2019, https://doi.org/10.4271/2019-01-1935.

[4] Gent, R.W., Dart, N.P. and Cansdale, J.T., *Aircraft icing*, Phil. Trans. R. Soc. Lond. A, 358, 2000.

[5] Wright, W., *User's manual for LEWICE version 3.2*, NASA/CR-2008-214255, 2008.

[6] Geuzaine, C., and Remacle, J.F.. *Gmsh: A 3-D finite element mesh generator with built-in pre-and post-processing facilities.*, Int. J. for Num. Methods in Engineering, 79(11):13091331, 2009.

[7] Makkonen, L., Stallabras ,J.R., Ice accretion on cylinders and wires. National Research council of Canada, NRC Tech. Report, TR-LT-005, 1984.

[8] Refloch, A., Courbet, B., Murrone, A., Villedieu, P., Laurent, C., Gilbank, P., Troyes, J., Tessé, L., Chaineray, G., Dargaud, J.B., Quémerais, E., Vuillot, F., *CEDRE Software*, Aerospace Lab Journal, Vol. 2, 2011.

[9] Courbet, B., Benoit, C., Couaillier, V., Haider, F., Le Pape, M.C., Péron, S., *Space Discretization Methods*, Aerospace Lab Journal, Vol. 2, 2011.

[10] Murrone, A., and Villedieu, P., *Numerical Modeling of Dispersed Two-Phase Flow*, Aerospace Lab Journal, Vol. 2, 2011.

[11] Rutard, N., Dorey, L.-H., Le Touze, C., and Ducruix, S., *Large-eddy simulation of an air-assisted liquid jet under a high-frequency transverse acoustic forcing*, International Journal of Multiphase Flow, Vol. 122, 2020, 10.1016/j.ijmultiphaseflow.2019.103144.

[12] Le Touze, C., Dorey, L.-H., Rutard, N., and Murrone, A., *A compressible two-phase flow framework for Large Eddy Simulations of liquid-propellant rocket engines*, Applied Mathematical Modelling, Vol. 84, pp. 265-286, 2020, 10.1016/j.apm.2020.03.028.

[13] Norde, E., Senoner, J.-M., van der Weide, E.T.A., Trontin, P., Hoeijmakers, H.W.M., and Villedieu, P. *Eulerian and Lagrangian Ice Crystal Trajectory Simulations in a Generic Turbofan Compressor*, Journal of Propulsion and Power, Vol. 35(1), pp. 1-15, 2018, 10.2514/1.B36916.

[14] Aupoix, B., *Roughness Corrections for the k-ω Shear Stress Transport Model: Status and Proposals*, Journal of Fluid Engineering, Vol. 137(2), 2015, 10.1115/1.4028122.

[15] Laurendeau, E., Bourgault-Ct, S., Ozcer, I., Hann, R., Radenac, E., Pueyo, A., Broeren, A., *Summary from the 1st AIAA ice prediction workshop*, AIAA AVIATION 2022 FORUM, 2022.

[16] Bragg, M.B., Yoshida, W., Broeren, A.P., Lee, S., and Woodard, B.S., *Ice Shape Classification for Swept Wings*, AIAA AVIATION 2020 FORUM, AIAA 2020-2845, 2020.